SCIENTIFIC COMMITTEE
THIRTEENTH REGULAR SESSION
Rarotonga, Cook Islands
9–17 August 2017

Exploratory geostatistical analyses of Pacific-wide operational longline CPUE data for WCPO tuna assessments

WCPFC-SC13-2017/SA-WP-03

L. Tremblay-Boyer[1], S. McKechnie, G.M. Pilling, J. Hampton

[1]Oceanic Fisheries Programme, The Pacific Community

Contents

Executive summary

A key feature of CPUE data is that catch rates tend to be uneven in space. This could be due to actual trends in abundance, which could relate to local environmental conditions, fishing fleets in specific locales using gear that increases catchability, low fishing effort in areas which give inaccurate average catch rates, oceanography conditions that increase catchability by, for instance, making fish more vulnerable to fishing gear (thermocline), or simply chance.

Geostatistical approaches to CPUE standardization have become more prevalent in recent years, due in part to improvements in algorithms which has made them more computationally efficient and the increased exposure in the fisheries literature. Geostatistics explicitly models the spatial structure in the response variable, that is, the fact that observations that occur closer in space are more likely to be similar.

The current paper presents an exploration of the potential of applying this method to WCPO longline operational data, and highlights both the benefits and some of the challenges. These analyses generated time series of standardised CPUE used as one-off CPUE sensitivities for the yellowfin and bigeye assessments, and also the regional weights used in other model runs of those assessments.

Basin-scale oceanographic information can be easily included within these models. When oceanography was included as part of the standardized indices, there was little difference in the index over time by region, though the regional weights did vary slightly by shifting some of the abundance towards region 1 where there is a clear thermocline feature. Comparison of the influence of oceanography variables on bigeye *vs.* yellowfin catch rates also underscores the challenges of disentangling the impacts of oceanography on catchability *vs.* abundance that emerge with the inclusion of this type of covariates in CPUE standardization.

There are a number of logistical advantages to the development of geostatistical approaches to standardize CPUE data in the WCPO. The Pacific-wide scale of the analysis makes it straightforward to generate standardized indices and measures of variations for different region configurations, unlike current standardization approaches which run on a discrete and isolated regional subset of the data and need to be relaunched when new regional structures are explored. The previously required extra step of calculating regional weights in a separate analysis can also be avoided since the model implicitly scales relative abundance among regions over time. The work presented here is an overview of ongoing research on this topic, which will be pursued collaboratively in the inter-sessional season. Moving forward, we identify four priority areas for development:

1. Modelling of the relationship between oceanography covariates and catch rates needs to be refined to ensure the model properly captures the spatio-temporal effect implied by oceanography cycles impacting the distribution of thermal layers differently across stock assessment regions.

2. Current diagnostics for this algorithm are limited and challenging to interpret at finer resolutions. The development of improved diagnostics which summarize model performance over covariate combinations should be prioritized, with a special attention to optimizing mesh configuration.

3. The indices required for WCPO assessments must be at the year-quarter scale, and the algorithm is currently configured such that the spatio-temporal interaction on the geostatistical surface matches that of the overall time effect used in the analysis. This might yield a

geostatistical surface that captures too much of the variation in the data, and dampens the abundance signal instead of clarifying it. Alternative approaches to parameterize the time interaction should be explored, for instance by constraining the knot × effect *via* an AR1 at the annual scale.

4. Continued exploration of alternative mesh configuration should be considered a priority, especially given edge effects in the WCPO for both the modelled variable and sampling intensity. Approaches to account for biased sampling intensity across the range of the response variable should also be considered.

We invite SC13 to:

- discuss the approach used here and the areas of potential development;
- discuss collaborative future work to enhance the analyses.

1 Introduction

Standardized indices of abundance from catch-per-unit-effort are an influential input in stock assessments as they provide the model with information on temporal trends in relative abundance. A key feature of CPUE data is that catch rates tend to be uneven in space. This could be due to actual trends in abundance, which could relate to local environmental conditions, fishing fleets in specific locales using gear that increases catchability, low fishing effort in areas which give inaccurate average catch rates, oceanography conditions that increase catchability by, for instance, making fish more vulnerable to fishing gear (thermocline), or simply chance. In addition, observations that occur closer in space are more likely to be similar (spatial autocorrelation), which makes it harder to distinguish the real signal of a spatial effect by an explanatory variable.

The simplest way to standardize against these spatial effects is to include a categorical cell effect in the GLM model, and indeed that is done in most WCPO CPUE standardizations (e.g. Campbell, 2004; McKechnie et al., 2017) and commonly in fisheries elswhere. However this approach incorporates a number of different influences within that effect and also assumes that nearby cells are independent from each other. There are some spatial effects that impact catchability, others that impact abundance. Ideally CPUE standardization would remove impacts of catchability but retain the abundance signal.

Geostatistical approaches to CPUE standardization have become more prevalent in recent years, due in part to improvements in algorithms which have made them more computationally efficient, and increased exposure in the fisheries literature (Thorson et al., 2015; Cao et al., 0; Shelton et al., 2014, see also Petitgas, 2001 for an earlier discussion). Geostatistics explicitly models the spatial structure in the response variable, that is, the fact that observations that occur closer in space are more likely to be similar. This allows the spatial autocorrelation to be removed, which increases the precision in estimates and makes it easier to identify a relationship between response and candidate explanatory variables.

The current paper presents an exploration of the potential of applying this method to WCPO longline operational data and highlights some of the challenges. These analyses generated one-off CPUE sensitivities for the yellowfin and bigeye assessments, and also the regional weights used in the diagnostic case.

The two main outputs of interest from this analysis are (1) standardized indices of abundance by region and (2) regional weights, so the results presented here focus on this. We note however that there are other potentially useful components produced by these models that are not directly covered in this paper.

2 Methods

Longline catch-per-unit-effort for bigeye and yellowfin was modelled using a delta-lognormal spatio-temporal GLM over the Pacific from 1960 to 2015. Standardized indices of abundance by stock assessment regions (cf. McKechnie et al., 2017) were extracted. The approach accounted for non-linear effects of temperature layers on catchability. The spatial effect was modelled using a geostatistical model, following the approach developed by Thorson et al. (2015) but with code adapted to include non-linear effects for oceanographical covariates, alternative mesh configurations, and Pacific transformation (see below). We give a brief overview of the approach here but direct readers to Thorson et al. (2015) and the R package (see below) for a fuller description of the approach.

2.1 Datasets

1. **Pacific-wide longline operational dataset:** The operational-level longline data set used in this analysis contains individual records of fishing activity, whereby on a given day and time a longline was set by a vessel in a particular location at the one degree resolution, and the numbers of fish caught of various species reported. The longline set itself would be characterized by a total number of hooks set and by the number of hooks that were set between each intermediate float deployed along the length of the line (hooks-between-floats or HBF). These intermediate floats are used to maintain the fishing gear at a particular depth in the water column. Catch by species in individuals were modelled for yellowfin and bigeye tuna. This dataset is further described in McKechnie et al. (2015). The data set, covering the entire breadth of the Pacific Ocean from around 45° N to 40° S and over sixty years of fishing (1952-2015) and both domestic and distant-water fishing fleets, comprised more than 10.5 million sets.
2. **Oceanography:** Sea temperature at depth profiles were obtained from the ECMWF ocean reanalysis system ORAS4 (Balmaseda et al., 2013 and see `www.ecmwf.int/en/research/climate-reanalysis/ocean-reanalysis`), which was the oceanography database extending the furthest back in time (1958) that was available at the time of the analysis. Values were mean-aggregated at the monthly x 1by1 cell resolution to match that of the operational dataset and further interpolated to convert from temperature at specific depths to depths for specific temperatures (see Figure 1). Based on existing knowledge of temperature preferences for bigeye and yellowfin tuna, the depth for temperature layers 12, 15, 18 and 20° C were computed, and an intermediate variable for the extent of the vertical habitat was defined as the depth difference (in meters) between the 12 and 18° C temperature layers. The general relationship between temperature layer depths and catch rates is shown in Figures 2 and 3.

2.2 Summary of geostatistical model

We used as a basis the R package SpatialDeltaGLMM developed by James Thorson (Thorson et al., 2015), available here: github.com/nwfsc-assess/geostatistical_delta-GLMM. We give a brief description of the model here but focus on describing features added or modified from the original algorithm.

The geostatistical surface ω_s was fitted assuming a Matern covariance matrix which is used to model the spatial autocorrelation, i.e. how the correlation between observations changes as distance between them increase, with anisotropy (which entails the relationship does not have to change in the same rate in all directions) and with a temporal interaction fitted as a random effect, $\epsilon_{s,t}$. The surface also requires the definition of knots s which are points where the effects are estimated (shape of the correlation surface between knots assumed to be piecewise linear). Each observation in the dataset then gets assigned to the knot which is the closest to them (see Figure 4). The ensemble of these knots are referred to as a mesh and can be configured to have different features, notably in how densely knots are distributed in edge areas (e.g. Figures 5 and 6).

Inclusion of oceanography splines: Data exploration highlighted the need to model oceanography covariates with a non-linear relationship. An additional investigation was the examination of incorporating oeanographic data. We used a zero-mean-constrained spline following the approach developed by Wood in the package mgcv (Wood, 2006), whereby the estimated spline is centered at zero for the model, which means it has no effect on the model intercept. This last feature was desirable as we aim to compare relative abundances across different model structures and these comparisons might be biased if intercept values are not kept constant across models. The design matrix for a zero-centered spline was defined here with three knots and using a b-spline as returned by the *s()* function in the mgcv package.

A delta-lognormal GLM was then fitted to the occurrence and catch rates observed for each set. The prediction for the response variable in their respective link space (binomial: logistic; positive: log), corresponding to observed set i, is:

$$P_i = \beta_t + \omega_s + \epsilon_{s,t} + f_1(i) + f_2(i)$$

whereby β is the year-quarter coefficient at t, ω is the coefficient estimated by the geostatistical surface for knot s (i.e. the knot to which observation i is the closest), ϵ is the time-interation effect for the geostatistical surface at time t, and f_1 and f_2 are the values for splines of two oceanographical covariates at observation i. Predictions of standardized abundance for i then excludes the value for the covariates linked to catchability, here the spline functions for oceanography variables, but otherwise retains the other predictors of density in space and time:

$$P_{k,t} = \beta_t + \omega_s + \epsilon_{s,t}$$

Density at knot k is then the product of back-transformed (R) binomial and positive effects:

$$D_{k,t} = R_{bino|k,t} \times R_{pos|k,t}$$

The overall year-quarter index is the sum of all densities at t weighted by the knot area:

$$I_t = \sum_{k=1}^{N_k} A_k \times D_{k,t}$$

All analyses were performed in R and GLMs were run with TMB (Kristensen et al., 2016) using

Parameter	Explanation
β_t	year effect
ω_s	static effect for the geostatistical surface
$\epsilon_{s,t}$	temporal effect for the geostatistical surface
f_1	continuous effect for first oceanography covariate
f_2	continuous effect for second oceanography covariate

algorithms developed in the libraries SpatialDeltaGLMM and INLA (Lindgren and Rue, 2015).

2.3 Definition of Pacific-wide coordinates

The construction of the geostatistical surface requires input data quantifying the distance between points. We used a two-point equidistant projection (*tpeqd*) to convert the longitude-latitude into coordinates where distance was represented correctly across all latitudes. This projection returns a coordinate system where distances are accurate from all points to two anchor points (Figure 7). We defined those two anchor points to be at the equator, and occur at longitudes located at the 33% and 66% quantile of the longitudes present in the dataset.

2.4 Subsampling

The large size of the longline datataset made it impractical to use it in its entirety for the algorithm to run in a reasonable time. The density of observations was much higher in the 20S to 20N region, and conversely reduced moving towards the poles. Since geostatistical approaches make the assumption that the value of the response variable is independent from the intensity of sampling, we elected to distribute evenly-spaced N_K knots in the dataset using a k-means algorithm on the extent of the surface covered by observations (see example for 100 and 200 knots under two mesh configurations in Figures 5, 8). An alternative would have been to distribute knots so that they represent effort densities (i.e. knots around the equator would have been closer together than in temperate areas) (see discussion at Pilling and Brouwer, 2017).

For exploration purposes to allow the model to run in under 1 hour, we used a very low subsampling rate where only 10,000 records were retained, but, unless otherwise mentioned, all models presented here had 500,000 records in the dataset (i.e. $\sim$ 0.05% sampling) with 200 knots under mesh configuration B (Figure 6). To select those sets out of the 10million sets + available, two subsampling schemes were explored: subsampling by flag, whereby the sampling rate was applied to retain even sampling across flags, and subsampling by knot, whereby the retained N records were distributed evenly across knots. This effectively resulted in a lower sampling rate for knots in highly fished areas, but allowed more observations to be retained at the edges of the distribution. It was also a way to reduce the violation of the model assumption that sampling rates are independent from the response variable (see above). All results presented here used the knot-subsampling approach, but preliminary results with the flag-subsampling approach were also presented to the SPC Pre-assessment workshop.

2.5 Standardized indices of abundance and regional weights

Following the equations described in Section 2.2, standardized indices of abundance used for the one-off sensitivities in the bigeye and yellowfin assessments were obtained by extracting all fitted effects for an observation except those that impacted catchability (i.e. the oceanography effects), back-transforming them and using their product following a standard delta-lognormal standardization approach. The index for a year-quarter for a region were the area-weighted sum of the standardized prediction for all cells in the region, and the standard error was extracted directly for year-quarter effects but otherwise left unadjusted between regions.

The area for each 1 degree cell was calculated *via* the PBSmapping package (Schnute et al., 2015) which calculates area by first converting coordinates into northings-eastings. These calculations tend to be accurate as long as the longitudinal span of observations is small, so we calculated area individually for each cell.

The regional weights for a species were calculating by aggregating area-weighted indices over a region for the period defined in the stock assessments as the scaling period (1980-1990), and standardizing so that the sum over all regions was equal to 1.

3 Results and discussion

Applying geostatistical methods on a dataset with the spatio-temporal span and size of that of the operational longline dataset used here is a non-trivial exercise with considerable methodological and computational challenges. To our knowledge none of the other recent applications of geostatistical models in fisheries science use a dataset matching this scale. The results presented here should thus be considered an initial overview, and will evolve as we further refine the methods used to apply this class of models to standardize WCPO catch rates. There are two parallel developments in the approach presented in this paper: 1) geostatistical methods and the exploration of algorithm settings on predictions (e.g. mesh configuration, subsampling, etc.); 2) the inclusion of oceanography covariates in the calculation of relative indices of abundance.

Starting with oceanography, there are pronounced temperature features across the WCPO which are likely to impact both tuna habitat and their vulnerability to fishing gear (Figure 1). For instance, the depth of the 15 degree layer is much shallower around the equator than in temperate assessment regions (see middle panel in Figure 1), which should increase the catchability of fish given sets performed at the same depth. A gradient in the depth of this temperature layer also occurs from east to west, which is thought to explain some of the higher catch rates for species like bigeye tuna in the EPO, and is also impacted by oceanography cycles such as El Niño (not shown here). All temperature layers clearly appear to relate to catch rates for both bigeye and yellowfin tuna (Figures 2 and 3). Here we picked 15 ° C as a compromise temperature that relates to both bigeye and yellowfin tuna preferences (Schaefer et al., 2007; Schaefer and Fuller, 2010), to explore the inclusion of oceanographic covariates in the model. We also included as a trial a measure of vertical temperature gradient based on the advice of the PAW (see bottom panel Figure 1). The shape of the relationship between catch rates and the binomial and lognormal component of the model as estimated as part of the geostatistical model is shown in Figure 9 (note the link-transformed axis). As expected from the observation of catch rates against this variable, it predicts maximum catch rates around a 15° thermal layer depth of just shallower than 200m for bigeye tuna and around 300m depth for yellowfin tuna. This might be due to the fact that a deeper 15° thermal layer

tends to be indicative of warmer sea surface temperatures, which also relates to higher yellowfin abundance. Since yellowfin tuna tend to occur at shallower depths than bigeye, it could be that their catchability is less influenced by the depth of the thermocline, and that the signal picked up by the model is instead caused by a correlation between the oceanography covariates used and other variables that impact yellowfin abundance. Disentangling the impacts of oceanography on catchability *vs.* abundance is probably the key challenge of accounting for oceanography covariates in CPUE standardization. In parallel, the shape also differs for the occurrence component of the model (i.e. binomial) with bigeye occurence in the catch becoming more common again at the higher thermocline depths. These contrasts between the yellowfin and the bigeye effects needs to be explored further. When oceanography was included as part of the standardized indices, there was little difference in the index over time by region (Figure 10 and 11), though the regional weights did vary slightly by shifting some of the abundance towards region 1 where there is a clear thermocline feature (see Figure 12 and 13, and also Figure 1).

Increasing the number of knots and observations led to little difference although, pending improved computer resources, we aim to further explore this axis (Figure 14 and 15). The one component that appeared to make a difference was the mesh configuration (Figure 16 and 17), possibly because it changed the distribution of knots in the region boundary areas. This area of the algorithm is a high priority for further exploration.

While there was a clear relationship predicted between vertical habitat and catch rates (Figure 9, it is unclear whether the effect is *via* catchability, abundance or purely correlational. The impact of including this variable in the standardization was more visible on the distribution of biomass over space than relative trends of abundance. Given that a temporal switch should be driven by changes in depth over time due to cyclical events like El Niño, a next step could be to split the model into subsets delineating regions where the distribution of the thermal layers varies over time (e.g. at the inter-annual scale) compared to ignoring this, to verify that the algorithm is properly parameterized to capture this effect.

Despite the methodological challenges, there are a number of logistical advantages to the development of geostatistical approaches to standardize CPUE data in the WCPO. The Pacific-wide scale of the analysis makes it straight-forward to generate standardized indices and measures of variations for different region configurations, unlike current standardization approaches which run on a discrete and isolated regional subset of the data and need to be relaunched when new regional structures are explored. The previously necessary extra step of calculating regional weights in a separate analysis can also be avoided since the model implicitly scales relative abundance between regions over time. The work presented here is an overview of ongoing research on this topic, which will be pursued collaboratively in the inter-sessional season. Moving forward, we identify four priority areas for development:

1. The modelling of the relationship between oceanography covariates and catch rates needs to be refined to ensure the model properly captures the spatio-temporal effect implied by oceanography cycles impcating the distribution of thermal layers differently across stock assessment regions.

2. Current diagnostics for this algorithm are limited and challenging to interpret at finer resolutions. The development of improved diagnostics which summarize model performance over covariate combinations should be prioritized, with a special attention to optimizing mesh configuration.

3. The indices required for WCPO assessments must be at the year-quarter scale, and the

algorithm is currently configured such that the spatio-temporal interaction on the geostatistical surface matches that of the overall time effect used in the analysis. This might yield a geostatistical surface that captures too much of the variation in the data, and dampens the abundance signal instead of clarifying it. Alternative approaches to parameterize the time interaction should be explored, for instance by constraining the knot × effect *via* an AR1 at the annual scale.

4. Continued exploration of alternative mesh configuration should be considered a priority, especially given edge effects in the WCPO for both the modelled variable and sampling intensity. Approaches to account for biased sampling intensity across the range of the response variable should also be considered (e.g. Diggle et al., 2010).

We also note that the availability of computing resources is a challenge especially given the size of the data set and limitations for analysing this dataset which by agreement requires it to be held on a single SPC server.

Finally, the PAW made a few suggestions for additional analyses we were not able to perform at this stage but should be prioritized in the inter-sessional period, notably the filtering of the dataset to only retain sets after 1980 where the oceanography model is of improved quality (this would also match the period where vessel identifiers are available throughout the dataset, thus allowing the inclusion of vessel effects in the standardization); and a formal comparison with 'conventional' GLMs where area × time interactions are modelled as discrete variables, to see how (whether) the shift to geostatistical approaches impacts indices obtained through this first, easier to apply method.

4 Acknowledgements

We thank James Thorson for making his code publicly available and creating a number of resources to facilitate the application of geostatistical approaches to fisheries dataset. We thank all CCMs for the provision of the operational data used in this analysis.

References

Balmaseda, M. A., Mogensen, K., and Weaver, A. T. (2013). Evaluation of the ecmwf ocean reanalysis system oras4. *Quarterly Journal of the Royal Meteorological Society*, 139(674):1132–1161.

Campbell, R. A. (2004). CPUE standardisation and the construction of indices of stock abundance in a spatially varying fishery using general linear models. *Fisheries Research*, 70:209–227.

Cao, J., Thorson, J. T., Richards, R. A., and Chen, Y. (0). Spatio-temporal index standardization improves the stock assessment of northern shrimp in the gulf of maine. *Canadian Journal of Fisheries and Aquatic Sciences*, 0(ja):null.

Diggle, P. J., Menezes, R., and Su, T.-l. (2010). Geostatistical inference under preferential sampling. *Journal of the Royal Statistical Society: Series C (Applied Statistics)*, 59(2):191–232.

Kristensen, K., Nielsen, A., Berg, C. W., Skaug, H., and Bell, B. M. (2016). TMB: Automatic differentiation and Laplace approximation. *Journal of Statistical Software*, 70(5):1–21.

Lindgren, F. and Rue, H. (2015). Bayesian spatial modelling with r-inla. *Journal of Statistical Software*, 63(19):1–25.

McKechnie, S., Tremblay-Boyer, L., and Harley, S. J. (2015). Analysis of Pacific-wide operational longline CPUE data for bigeye tuna. WCPFC-SC11-2015/SA-WP-03, Pohnpei, Federated States of Micronesia, 5–13 August 2015.

McKechnie, S., Tremblay-Boyer, L., and Pilling, P. (2017). Background analyses for the 2017 stock assessments of bigeye and yellowfin tuna in the western and central Pacific Ocean. WCPFC-SC13-2017/SA-IP-06, Rarotonga, Cook Islands, 9–17 August 2017.

Petitgas, P. (2001). Geostatistics in fisheries survey design and stock assessment: models, variances and applications. *Fish and Fisheries*, 2(3):231–249.

Pilling, G. and Brouwer, S. (2017). Report from the spc pre-assessment workshop, noumea, april 2017. Technical Report WCPFC-SC13-2017/SA-IP-02, Rarotonga, Cook Islands, 9–17 August 2017.

Schaefer, K. M. and Fuller, D. W. (2010). Vertical movements, behavior, and habitat of bigeye tuna (thunnus obesus) in the equatorial eastern pacific ocean, ascertained from archival tag data. *Marine Biology*, 157(12):2625–2642.

Schaefer, K. M., Fuller, D. W., and Block, B. A. (2007). Movements, behavior, and habitat utilization of yellowfin tuna (thunnus albacares) in the northeastern pacific ocean, ascertained through archival tag data. *Marine Biology*, 152(3):503–525.

Schnute, J. T., Boers, N., and Haigh, R. (2015). *PBSmapping: Mapping Fisheries Data and Spatial Analysis Tools*. R package version 2.69.76.

Shelton, A., Thorson, J., Ward, E., and Feist, B. (2014). Spatial semiparametric models improve estimates of species abundance and distribution. *Canadian Journal of Fisheries and Aquatic Science*, 71():1655–1666.

Thorson, J., Shelton, A., Ward, E., and Skaug, H. (2015). Geostatistical delta-generalized linear mixed models improve precision for estimated abundance indices for West Coast groundfishes. *ICES Journal of Marine Science*, 72(5):1297–1310.

Wood, S. N. (2006). *Generalize Additive Models: An introduction with R*. Chapman and Hall/CRC.

5 Figures

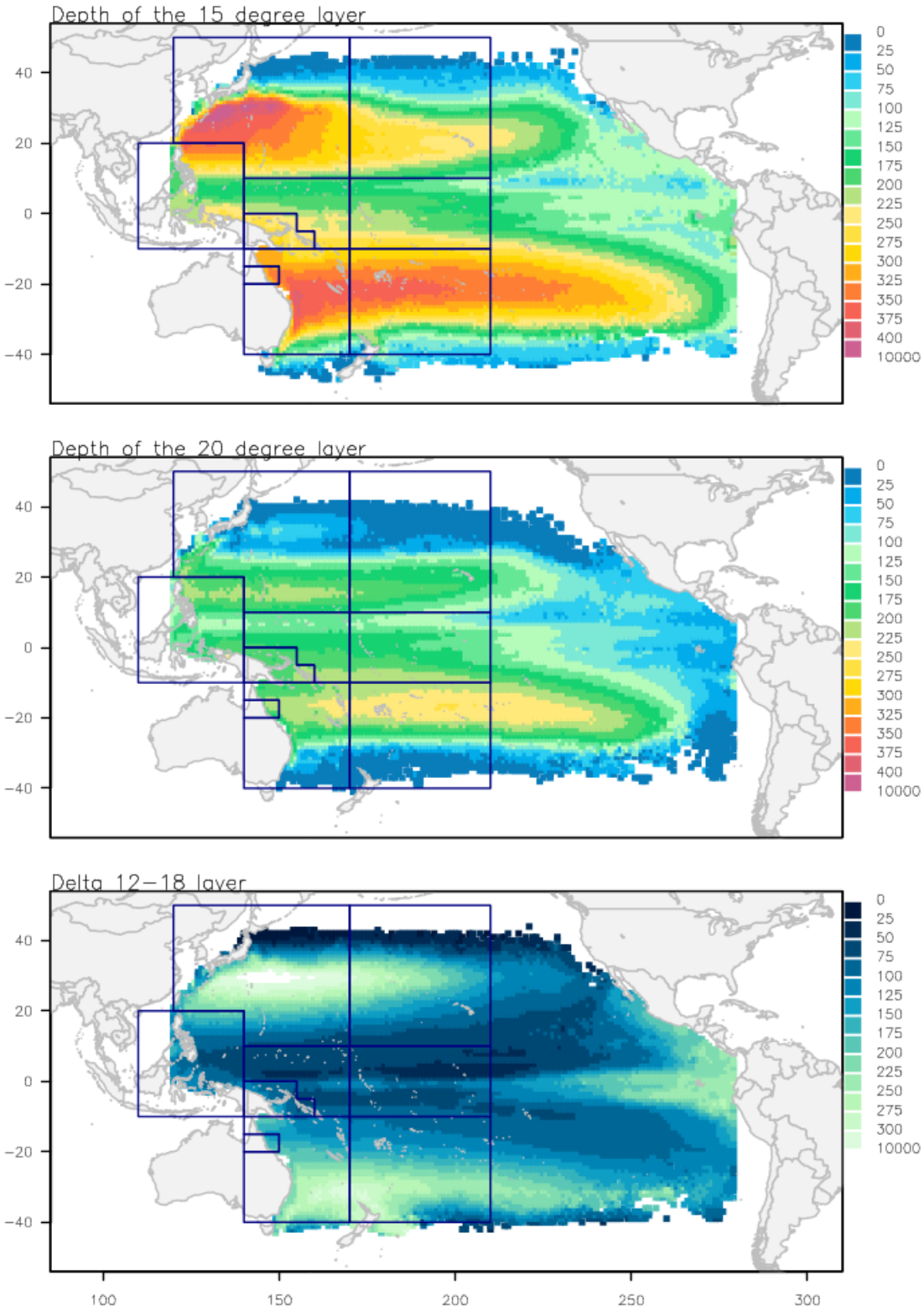

Figure 1: Key oceanography variables with 2017 updated region structure for the bigeye and yellowfin assessments.

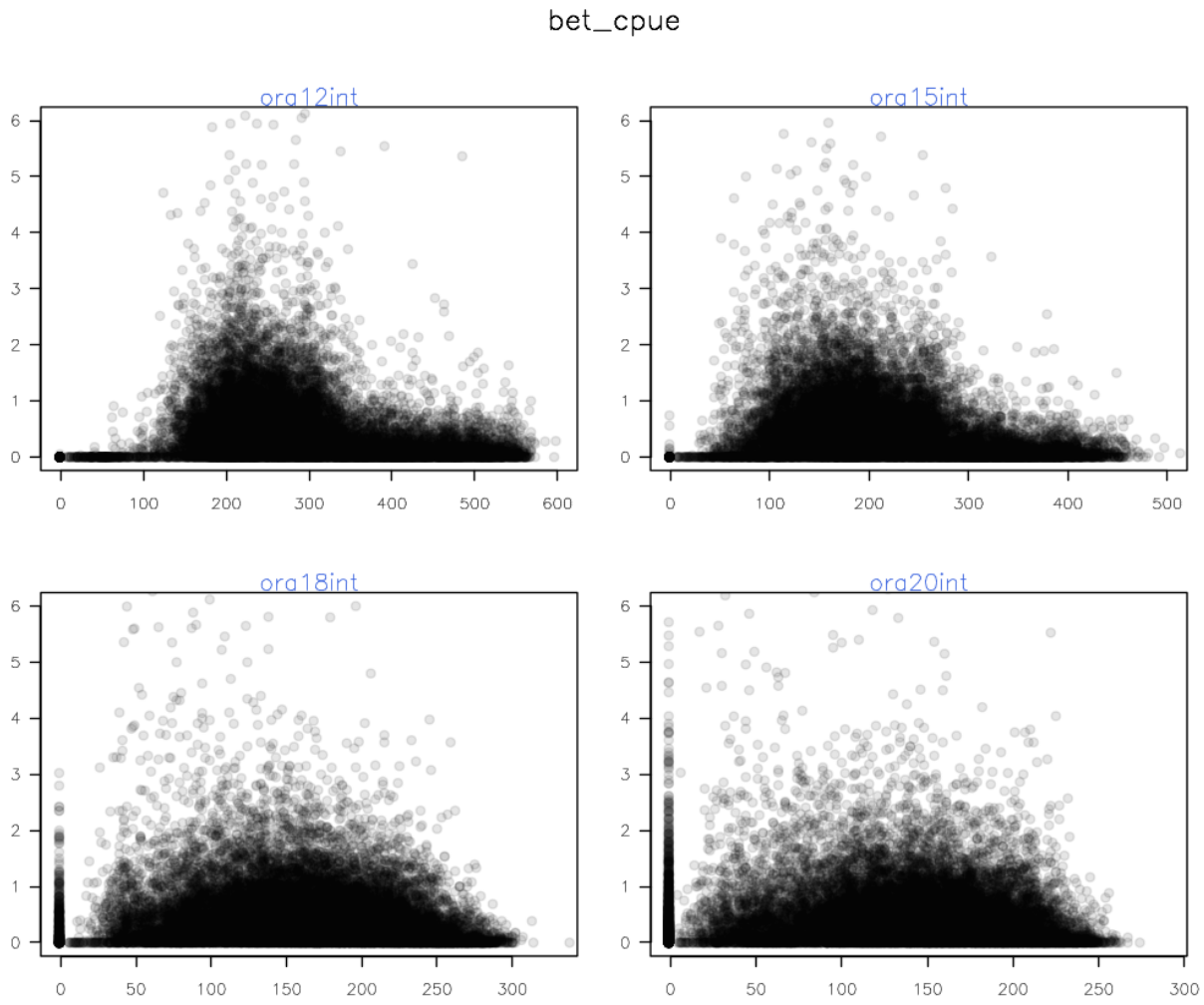

Figure 2: Relationship between bigeye tuna catch rates and various temperature layer depths.

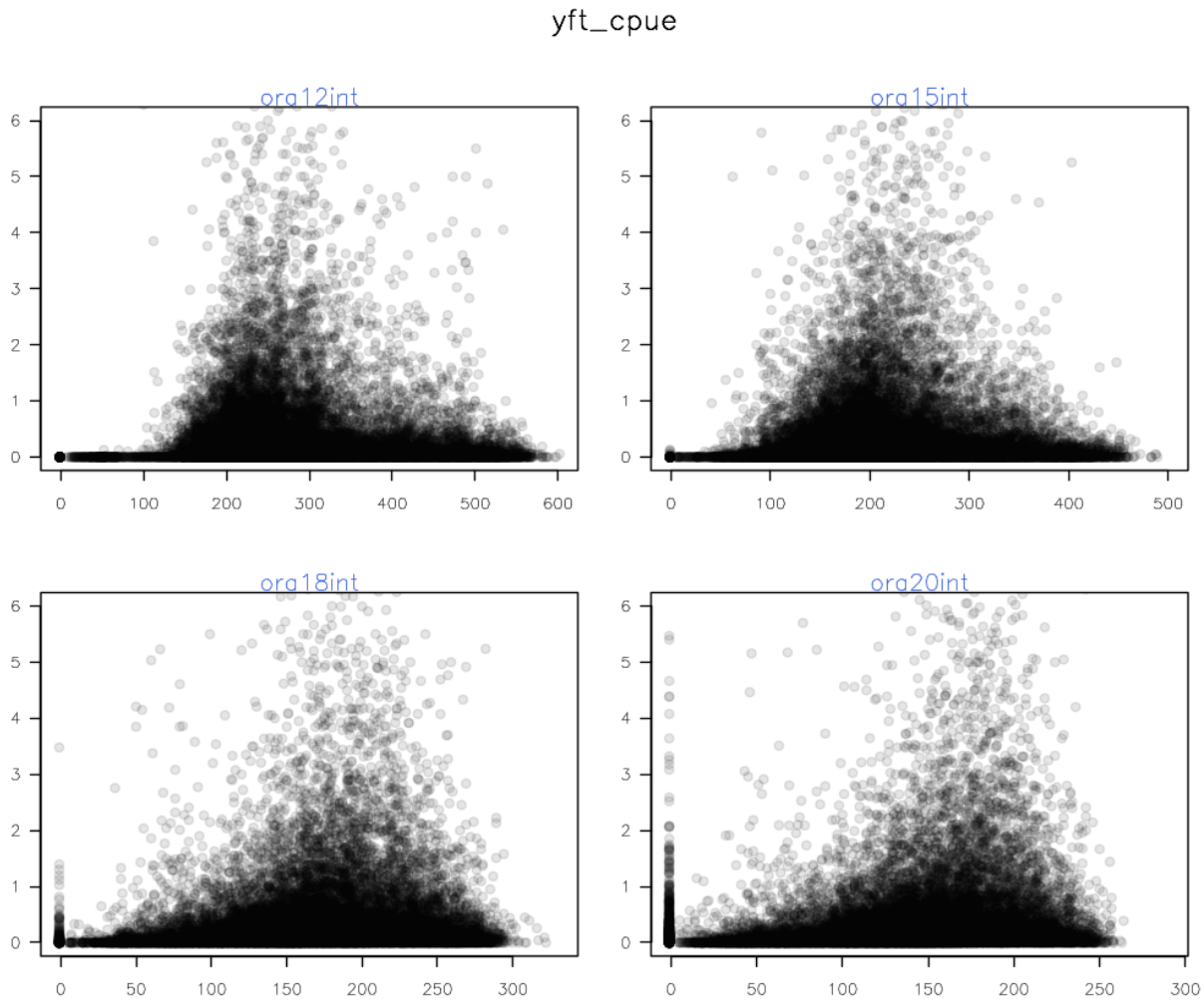

Figure 3: Relationship between yellowfin tuna catch rates and various temperature layer depths.

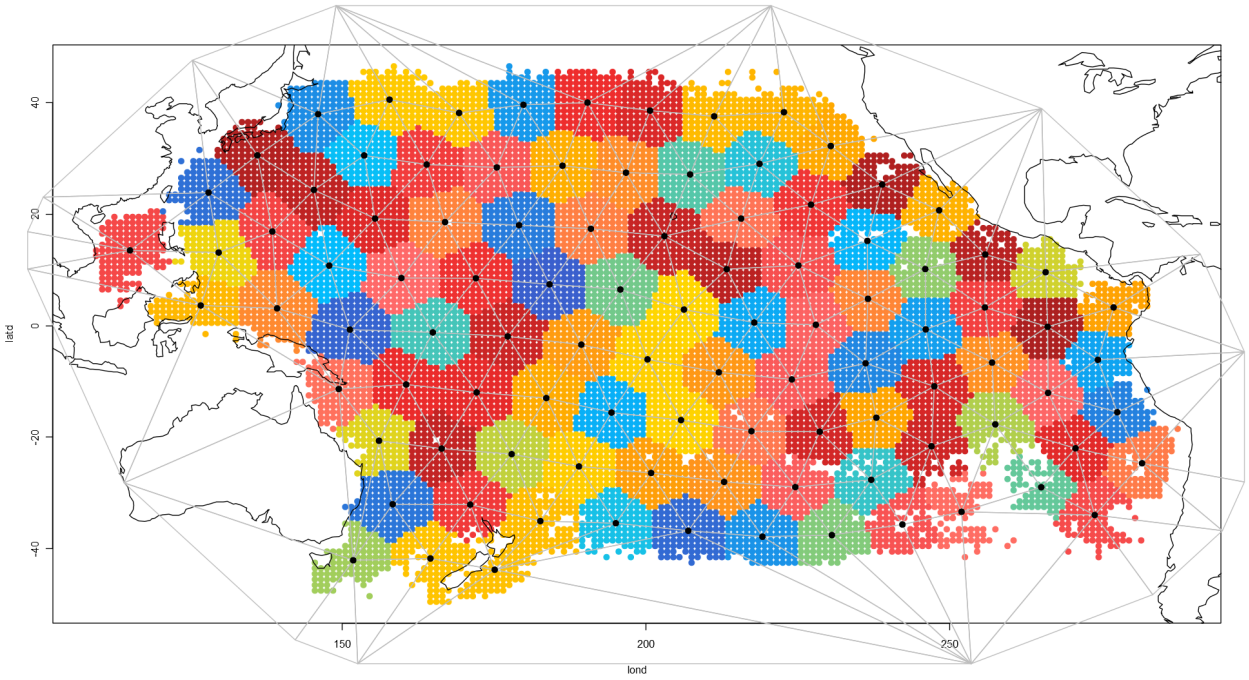

Figure 4: Diagram of knot assignment by point: the geostatistical surface gets estimated at each knot value, and each 1×1 cell in the dataset gets assigned the value estimate for the knot closest to it. Here points assigned to a specific knot share the same colour.

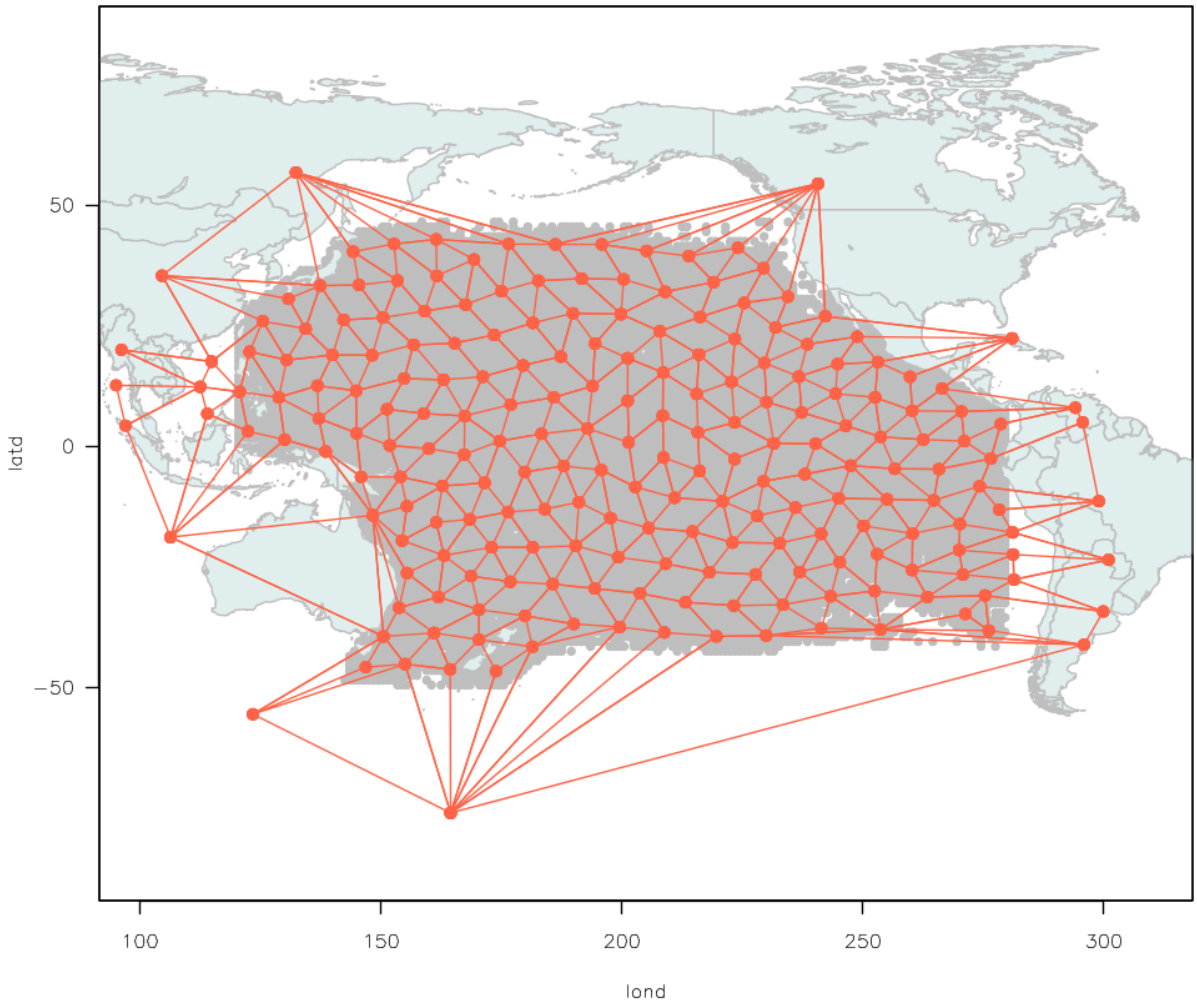

Figure 5: Mesh configuration A: 200 knots for the observed area, low knot density at the edges.

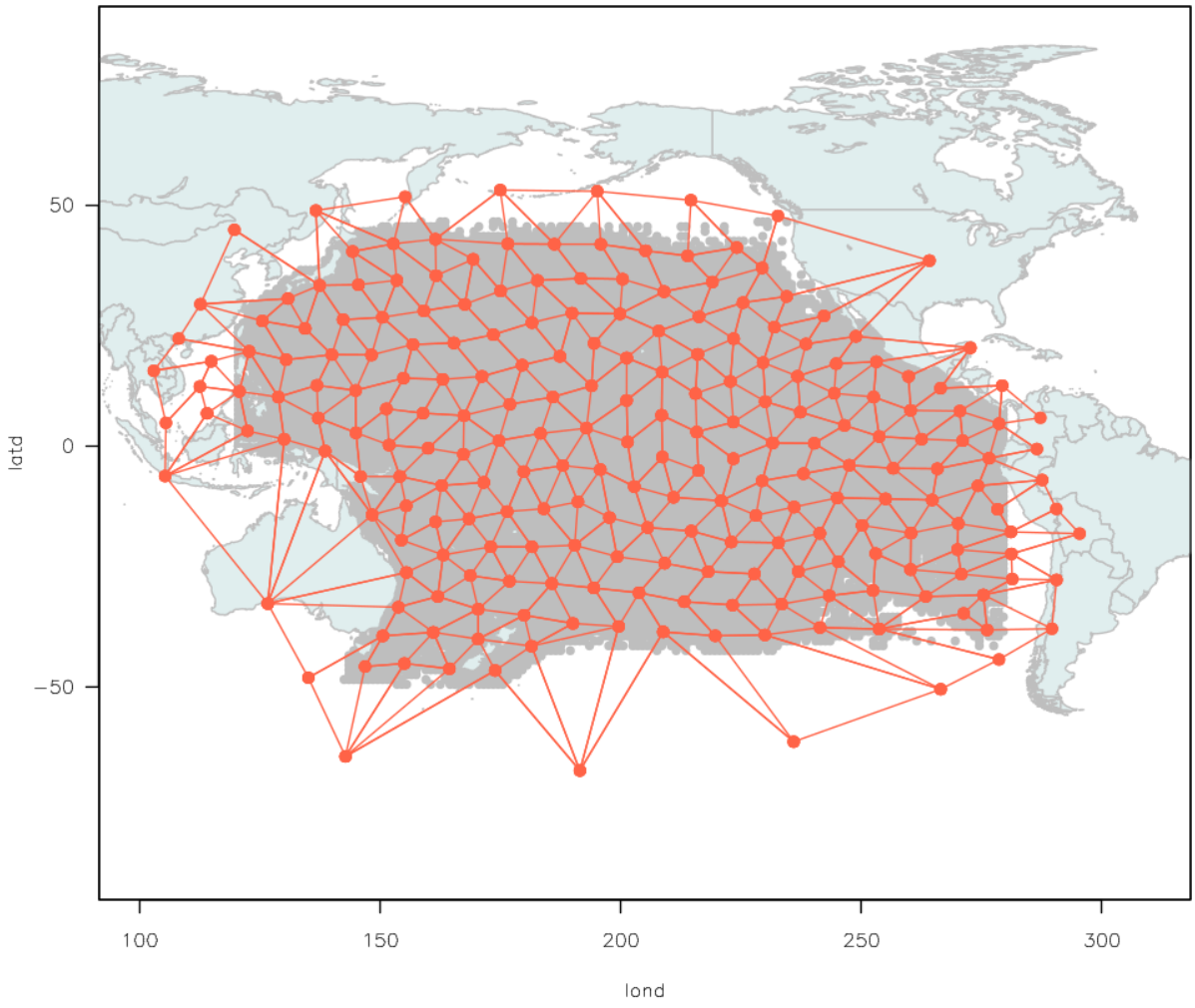

Figure 6: Mesh configuration B: 200 knots over the observed area, higher knot density in the edges.

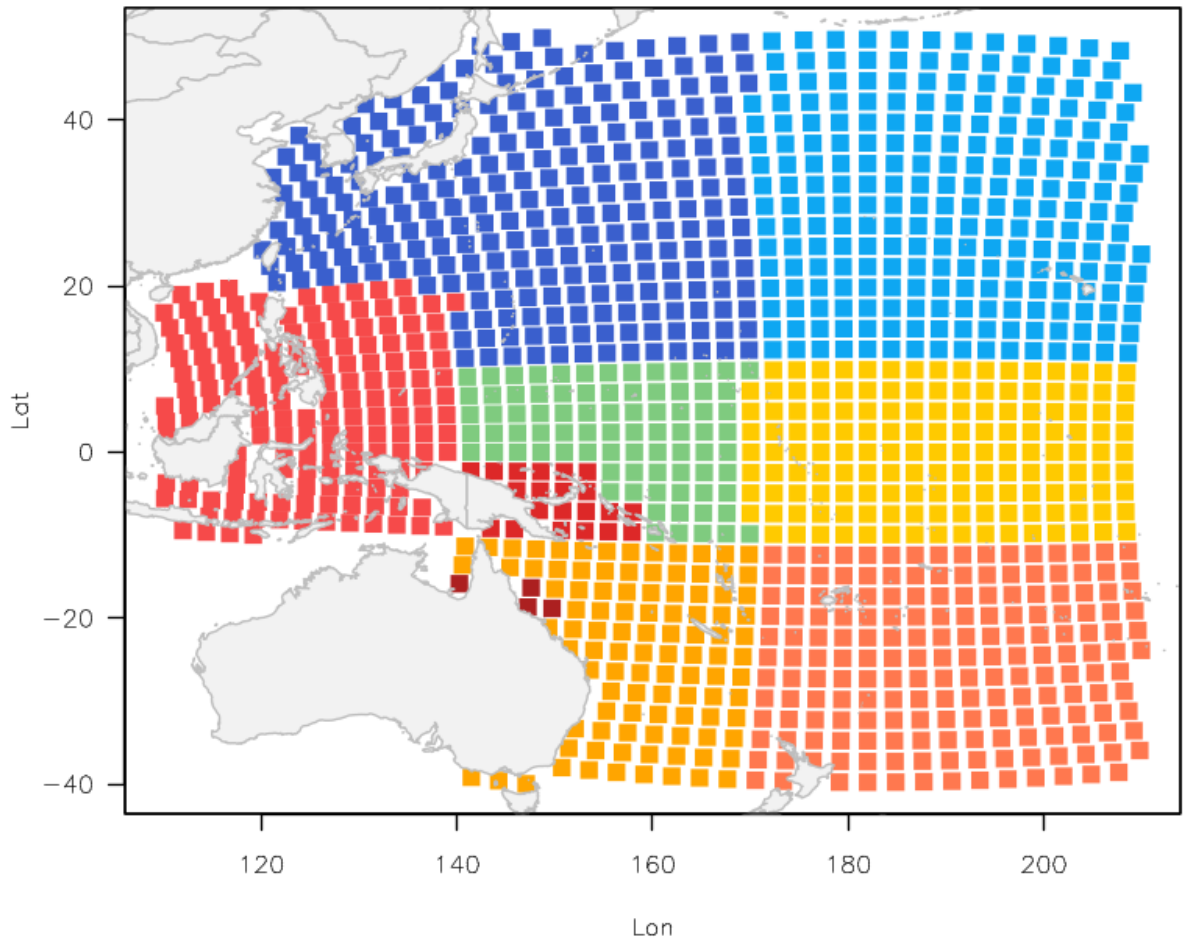

Figure 7: 5×5 Pacific coordinates back-transformed from *tpeqd* projection with the 2017 bigeye and yellowfin assessment regional structure highlighted.

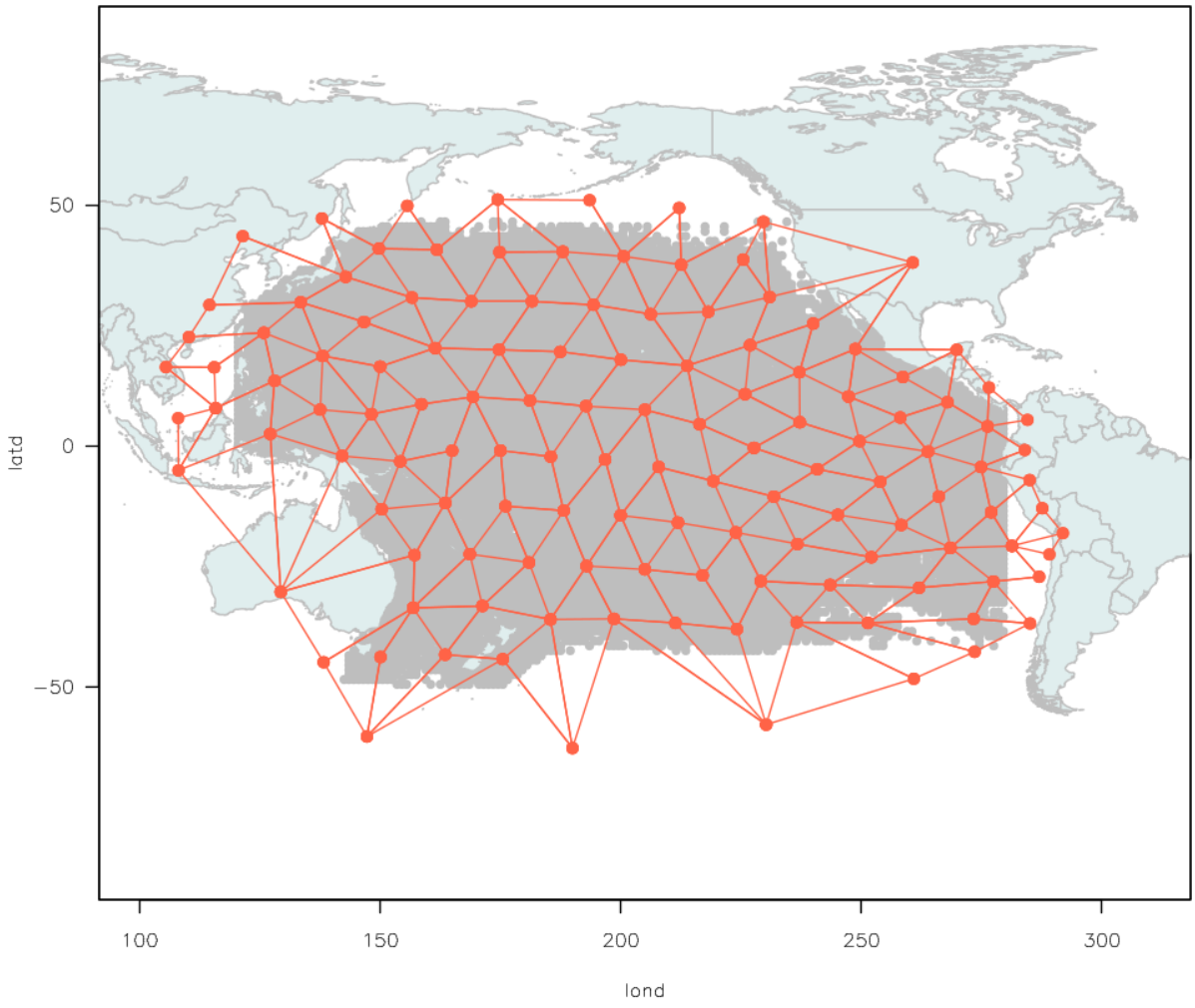

Figure 8: Mesh configuration used for exploratory models: 100 knots, low knot density at the edges.

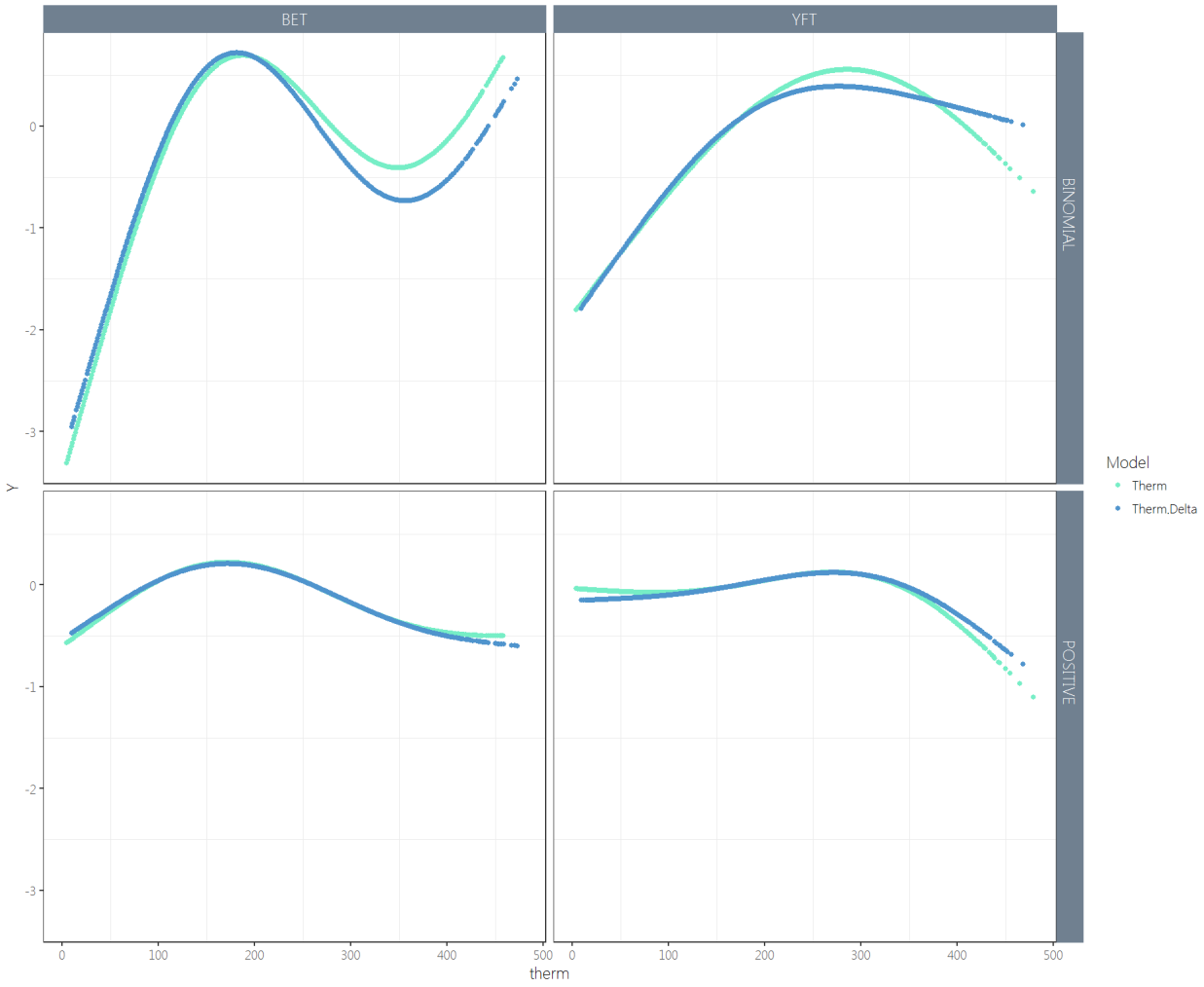

Figure 9: Fitted effect of the 15th degree layer on BET and YFT catch rates, with and without the inclusion of the additional delta 12-18 ° C layer, and for the binomial and lognormal components of the model.

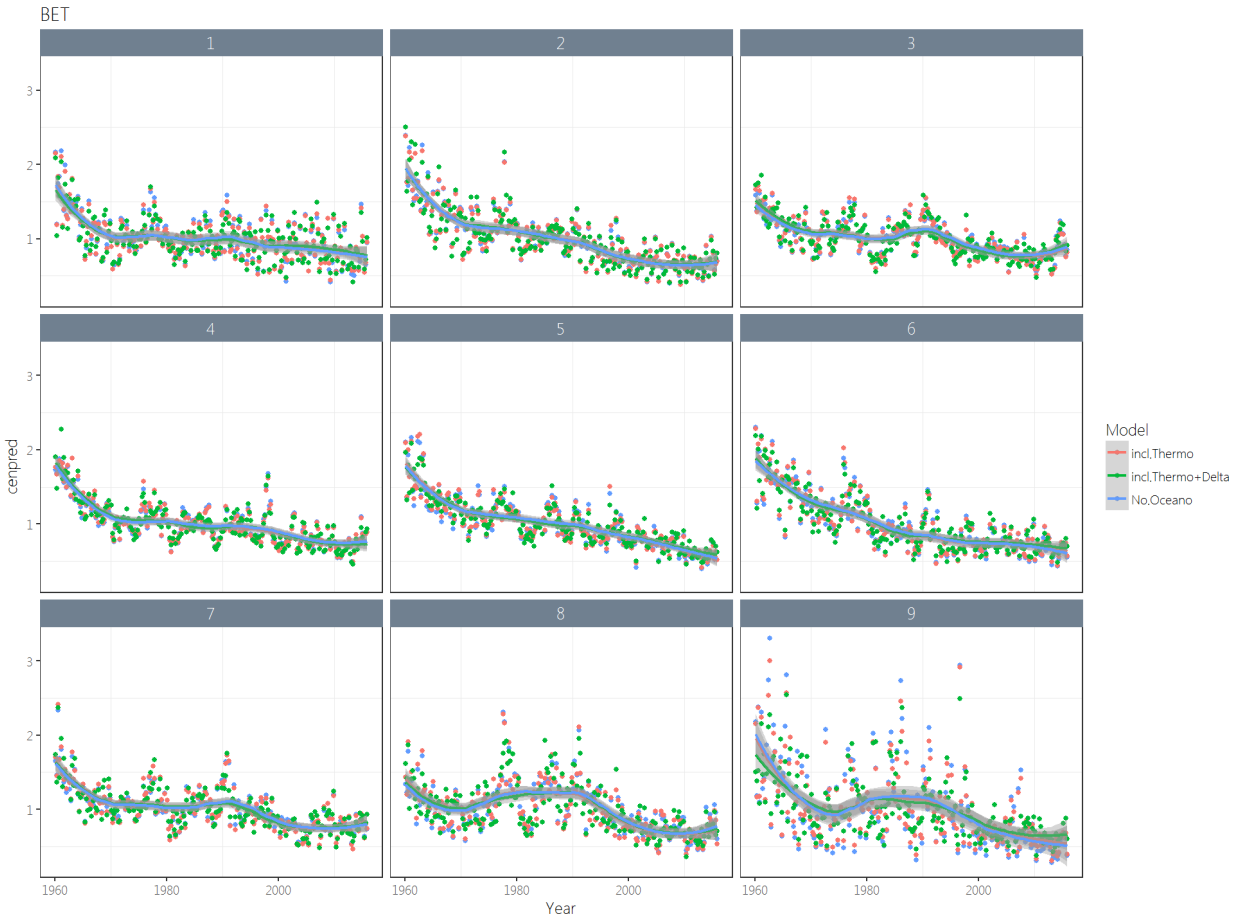

Figure 10: Comparison of BET mean-centered standardized abundance indices when one or two oceanography covariates are added to the standardization.

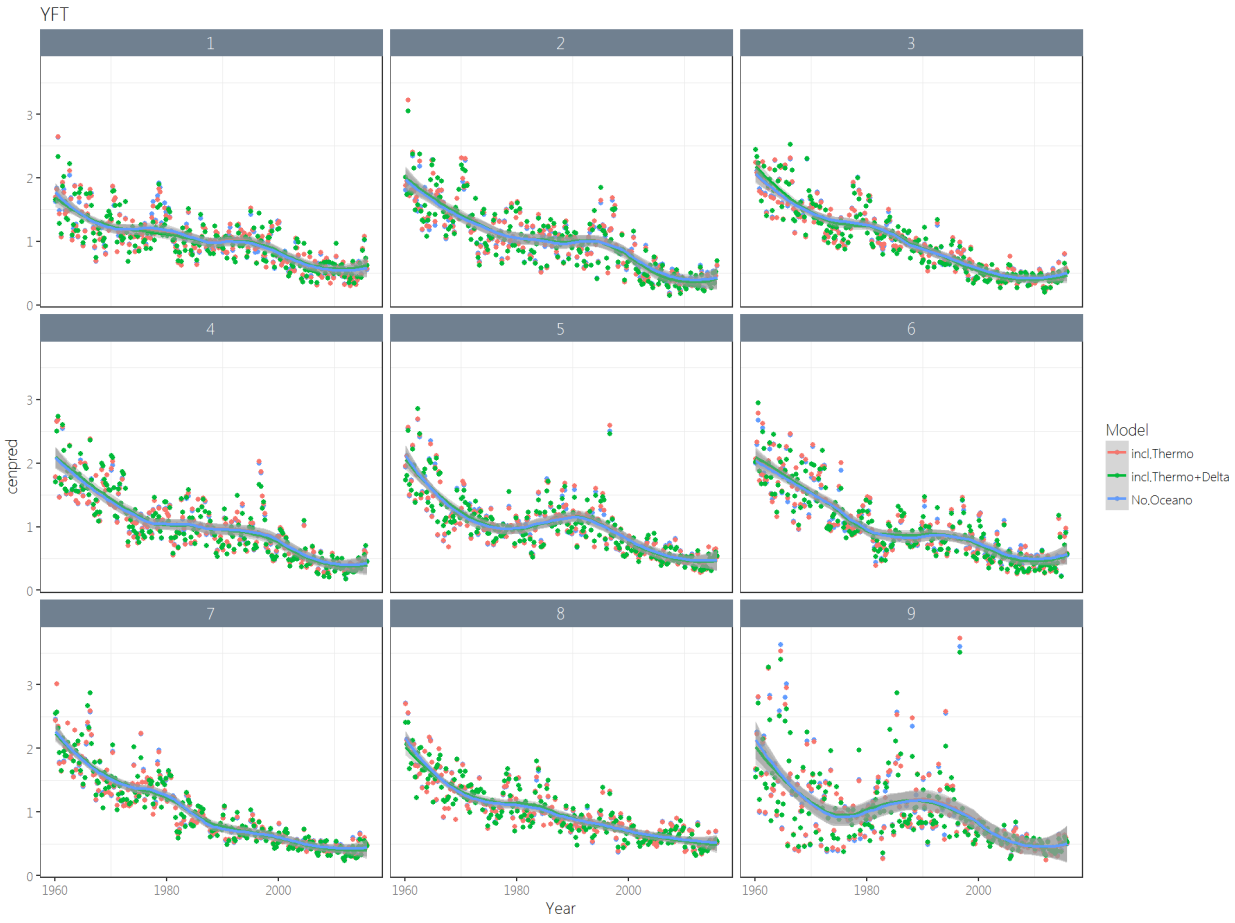

Figure 11: Comparison of YFT mean-centered standardized abundance indices when one or two oceanography covariates are added to the standardization.

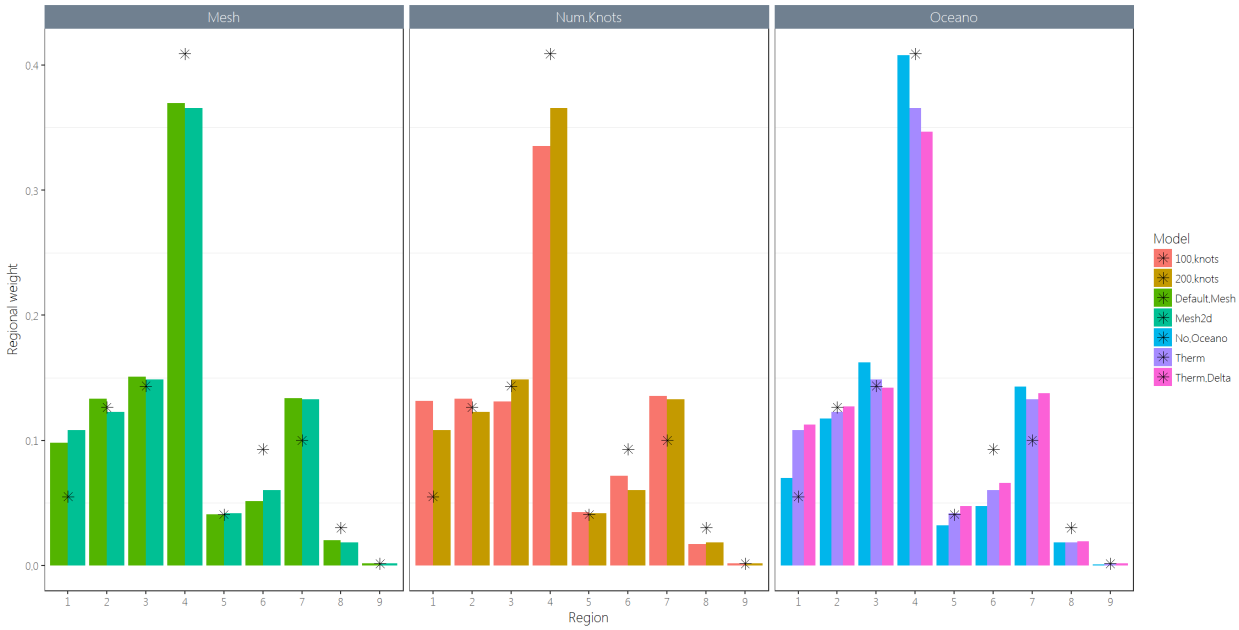

Figure 12: BET comparison for regional weights

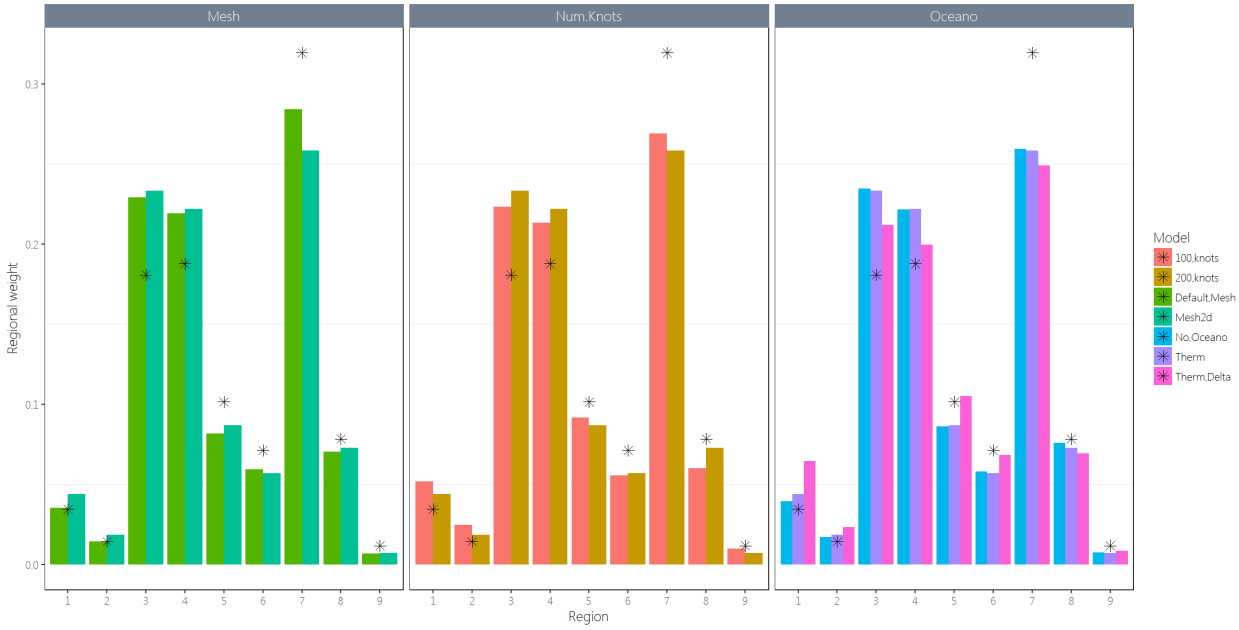

Figure 13: YFT comparison for regional weights

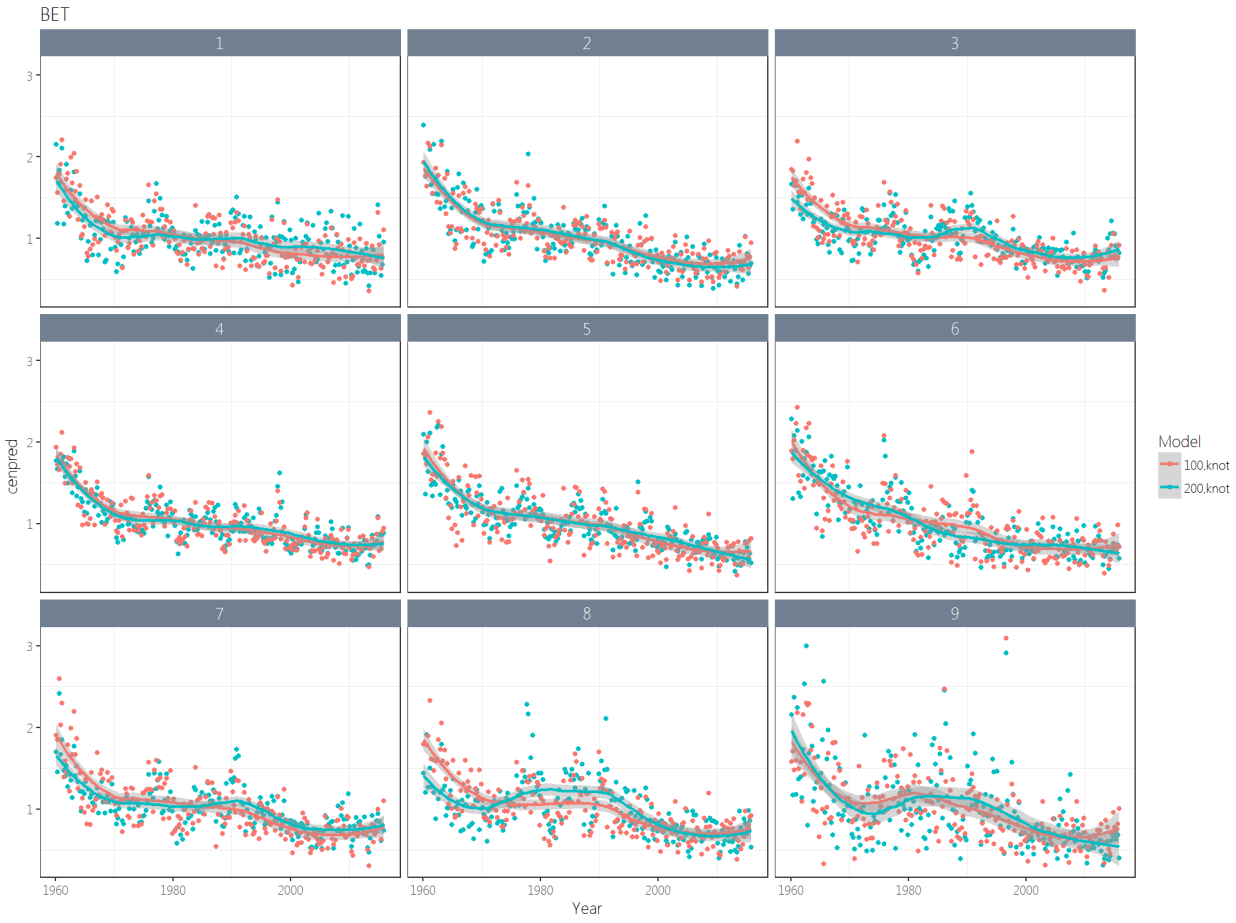

Figure 14: Comparison of BET mean-centered standardized abundance indices under different knot configurations.

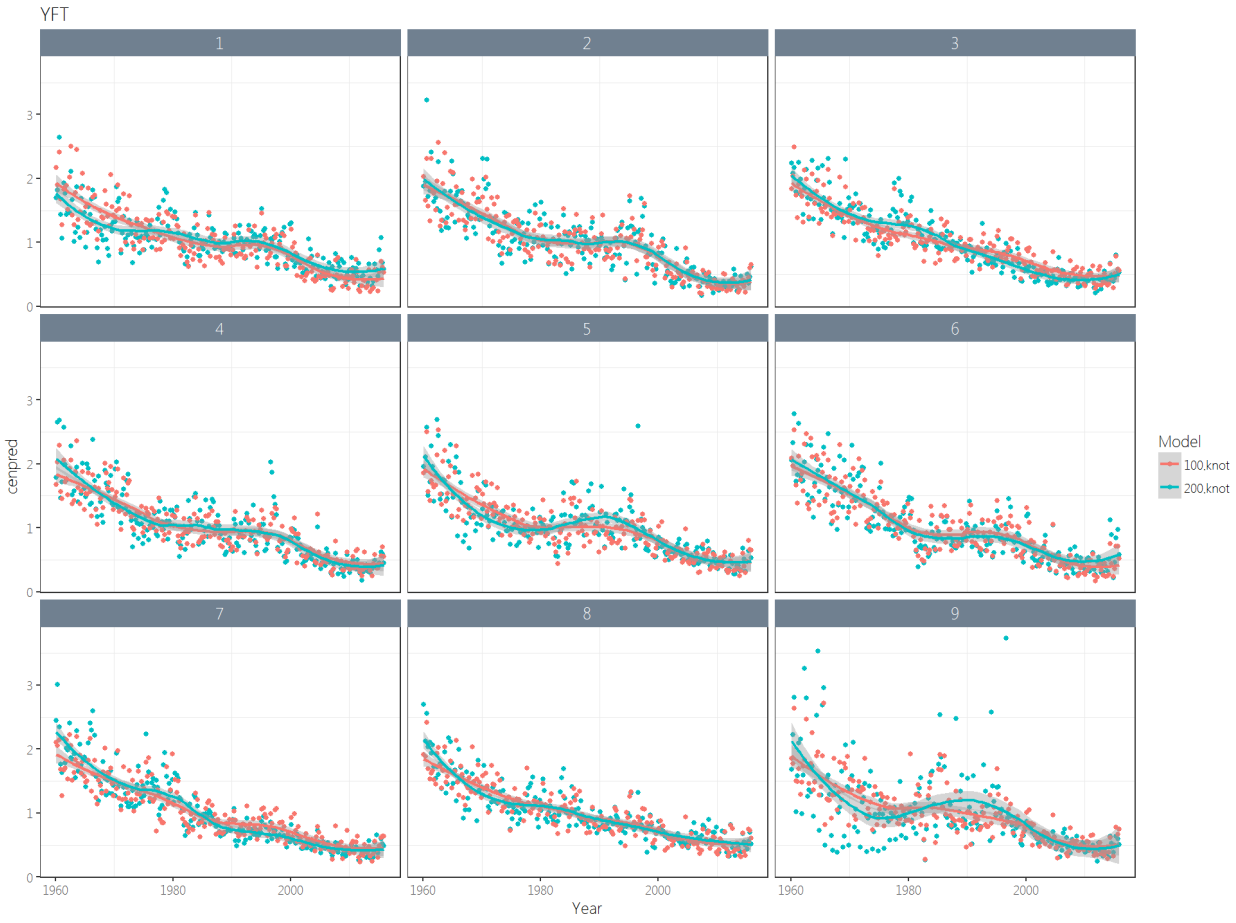

Figure 15: Comparison of YFT mean-centered standardized abundance indices under different knot configurations.

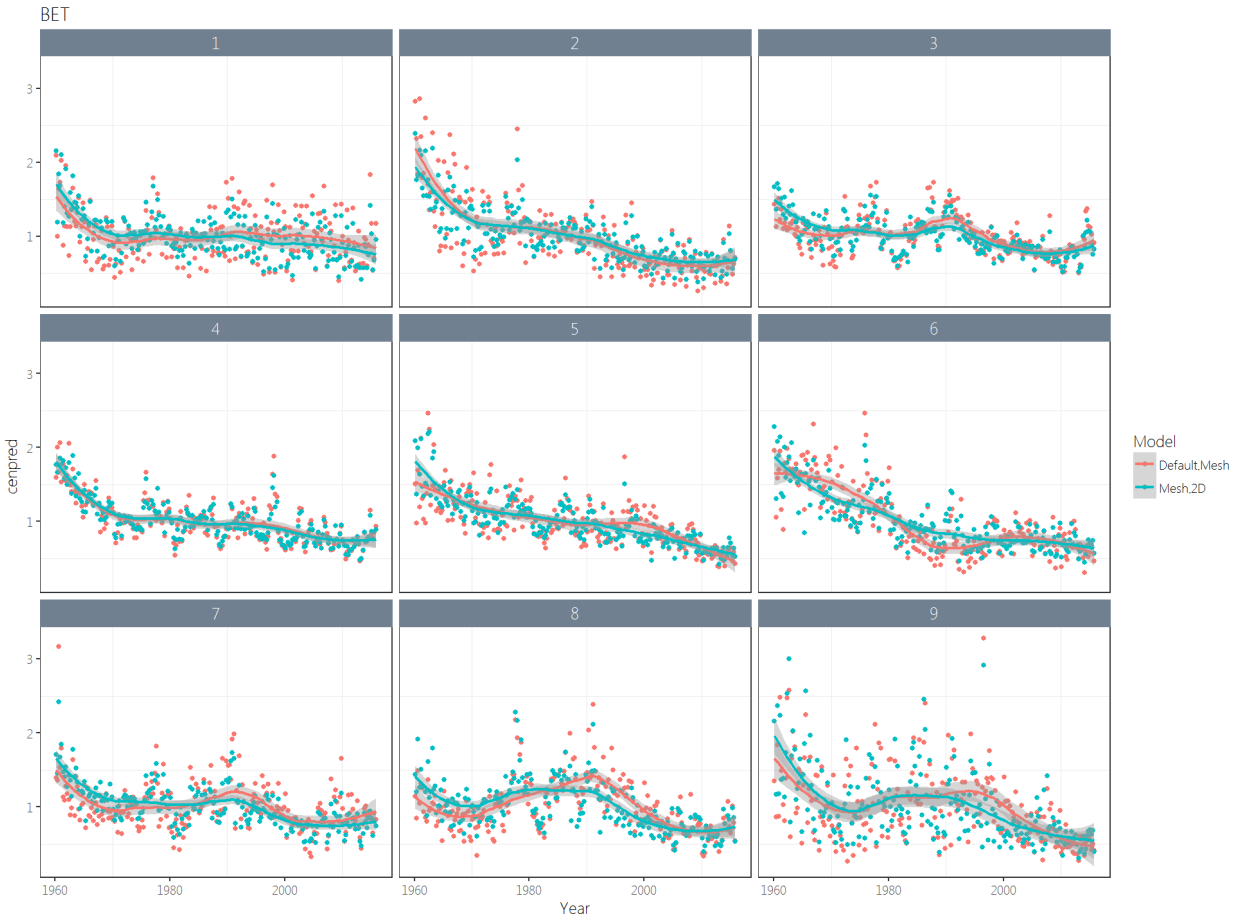

Figure 16: Comparison of BET mean-centered standardized abundance indices under different mesh configurations.

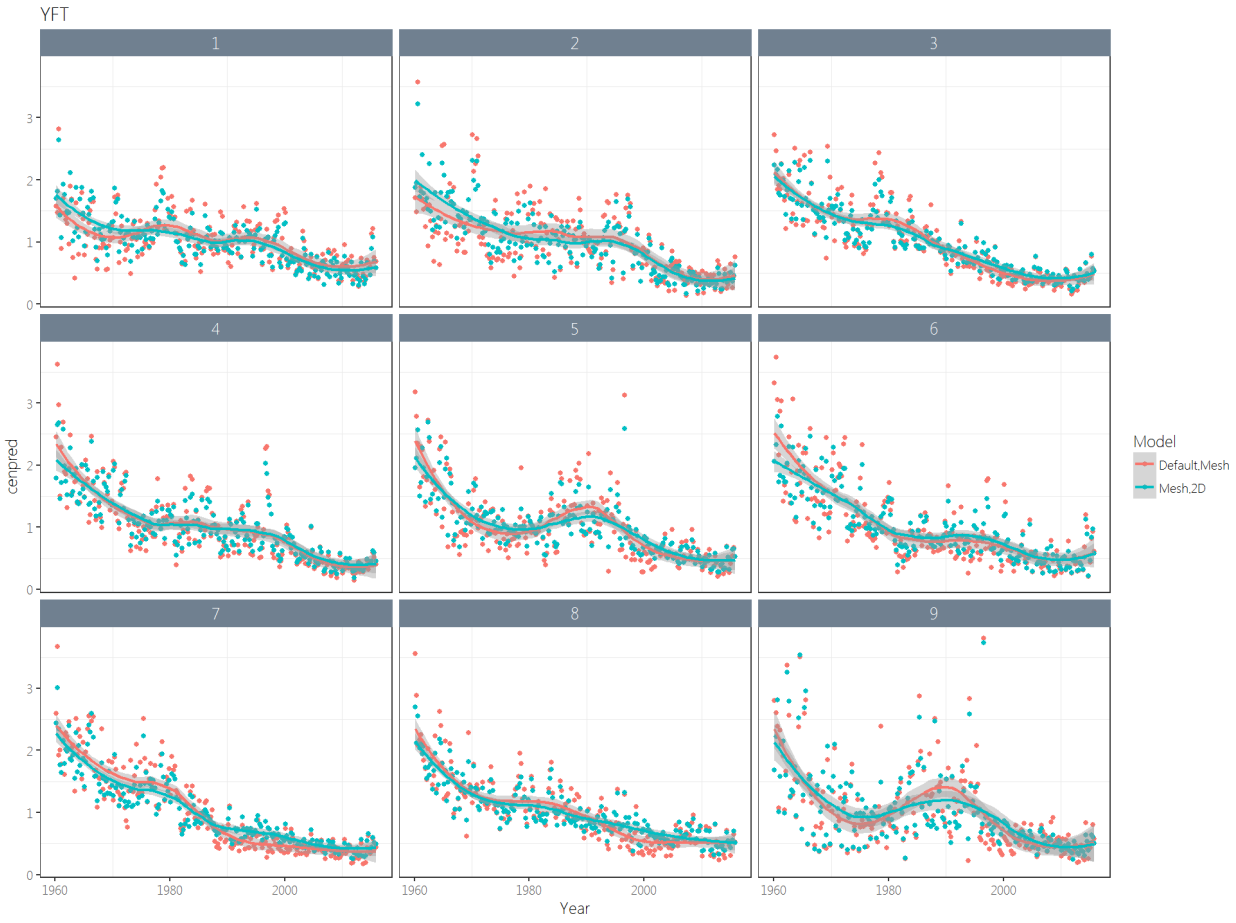

Figure 17: Comparison of YFT mean-centered standardized abundance indices under different mesh configurations.